Effect of growth pressure on InGaN quantum well optical and structural properties

A. V. Sakharov[1], A. F. Tsatsulnikov[1], W. V. Lundin[1], A. E. Nikolaev[1], E. E. Zavarin[1], S. O. Usov[1,2], M. J. Hÿtch[3], and N. Cherkashin[3]

[1]*Ioffe Institute 194021, Politechnicheskaya 26, St-Petersburg, Russia*

[2]*Submicron Heterostructures for Microelectronics, Research & Engineering Center, RAS 194021, Politechnicheskaya 26, St-Petersburg, Russia*

[3]*CEMES-CNRS/Université de Toulouse, 29 rue Jeanne Marvig, F-31055 Toulouse, France, 31055, Toulouse, France*

[*]E-mail: val@beam.ioffe.ru

Abstract

Here, we study the effect of pressure during metalorganic vapor phase epitaxy of InGaN/GaN quantum wells (QWs) on their luminescent and structural properties using photo- and electroluminescence spectroscopy and transmission electron microscopy. The QWs grown at "standard" low pressure of 100 mbar were found in form of two-dimensional layers of constant thickness and composition. We show that a growth at elevated pressures, in the range of 200-1000 mbar, stimulates the formation of islands. Two principal regimes of InGaN formation at elevated pressures were revealed. A growth at moderate pressures leads to the formation of islands of an increased indium content and thickness and, thereby, to a broadening of emission spectrum and a long wavelength shift of its peak position with respect to that of the "standard" structure. A growth at too high pressures hampers indium incorporation into islands and leads to the formation of additional dislocations in the active regions. A QW growth at optimal elevated pressure allows the longest wavelength emission with the maximal efficiency of light emitting diode structures. We show that an optimal pressure is specific to the given growth system.

Keywords : InGaN, MOVPE, pressure, LED

Introduction

Pressure in a reactor plays an important role during growth of III-N semiconductors by metal-organic vapor phase epitaxy (MOVPE) as it influences the precursor transport to a wafer surface and chemical reactions on a surface and in the gas phase. An increase in the reactor pressure during GaN growth is known to improve material and device properties as reported for laser structures [1]. Several authors report a reduction of the dislocation density in GaN layers grown at elevated pressure [2, 3]. A change in reactor pressure has also an impact on the impurity incorporation in GaN. The impurity concentrations were found to decrease with increasing growth pressure and ammonia flow [4-6].

For InGaN growth, the influence of pressure is much more complex than for GaN. An optimum growth of InGaN material is carried out at temperatures lower than that used for GaN material [7]. A tendency for the easier InN decomposition at elevated temperatures is suppressed by an increase in the reactor pressure, in particular, by an increase in both NH_3 and TMIn partial pressures [7, 8]. Therefore, pushing the upper limits of pressure towards higher values, a growth of InGaN material at higher temperatures and, thus, of a better quality, would be possible.

A theoretical analysis of InGaN growth at elevated pressure gives the contradictory results. The thermodynamic analysis of InGaN growth, applied for a relaxed material, predicts a maximum solubility of In in GaN of less than 6% at temperature of 800°C [9] while some other calculations show that, assisted by strain, the growth of homogeneous $In_xGa_{1-x}N$ thin films of indium composition up to 50% should be possible [9, 10].

However, one would expect an enhanced gas-phase condensation of In vapor on a wafer surface at elevated pressures that can hamper effective indium incorporation into layers and, thus, disable the formation of high indium content layers. Moreover, a formation of gallium adducts is expected due to gas-phase parasitic reactions amplifying at elevated pressures. This phenomenon could lead to a reduction in the InGaN growth rate and, possibly, to a reduction in the material quality (this problem has not been well studied yet).

Few experiments on InGaN growth at above-atmospheric pressure [12] support the model predictions described in [10]. On the other hand, typical pressure applied during InGaN growth is contained within the range of 100-1000 mbar which is limited by the given growth system. Data reported for the influence of pressure, from this range of values, on the growth of thin InGaN/GaN quantum wells (QWs) are rather contradictory: some papers report an increase in In content in InGaN layers [13, 14], while some others demonstrate a hampering of indium incorporation into layers [15-17] grown at elevated pressures. Interesting to note that an increase and a decrease in In content with pressure are reported for horizontal/planetary and vertical growth systems, respectively. Most of these papers evidence a tendency for a phase separation in InGaN layers at elevated pressures and an existence of some optimum pressure in terms of luminescence efficiency of the structures.

In this paper, we report on a systematic study of the effect of growth pressure on optical and structural properties of InGaN QW structures grown in horizontal and planetary growth systems.

Experiment

Epitaxial structures were grown by metalorganic vapor phase epitaxy (MOVPE) using standard planetary reactor AIX2000HT epi-system and home developed Dragon-125 system with a horizontal-flow reactor. Both reactors were equipped with *in-situ* optical reflectance monitoring (ORM) systems for a precise growth control. Samples were grown on (0001) sapphire substrates.

The samples dedicated for optical investigations contain an InGaN/GaN short-period superlattice (SPSL), a low temperature grown GaN barrier and three InGaN quantum wells (QWs) subjected to growth interruptions (GIs) after their deposition. Growth pressure was varied from 100 mbar to 1000 mbar. To reveal the effect of pressure, the structures differ one from another only by reactor pressure during growth of InGaN/GaN QWs.

Light emitting diode (LED) samples contain the similar active region sandwiched between n- and p-doped cladding layers. The details on the growth of such structures can be found in [18]. Two sets of LED structures were grown in different growth systems: Aixtron 2000HT and Dragon 125. A structure design of the samples grown in two epi-systems was identical and similar growth regimes were applied.

All structures were studied by various characterization methods including transmission electron microscopy, photoluminescence (PL) and electroluminescence (EL) spectroscopy. The PL investigations allowed estimating a PL spectrum peak position, its full width on a half maximum (FWHM) and its integral intensity as function of recording temperature in the range from 10K to 300 K. Electroluminescence investigations were carried out on a wafer with an area of about 0.4 mm^2 using indium contacts. A peak position and a FWHM of the EL spectra as well as external quantum efficiencies (EQE) of the LED structures have been extracted.

Weak beam dark field imaging has been applied for a structural quality characterization of the samples. The experiments were performed at 200 kV in the Jeol 2010 microscope.

Geometric Phase Analysis (GPA) [19] of high resolution transmission electron microscopy (HRTEM) images was applied to map strain with a subnanometer spatial resolution allowing extracting an alloy composition and thickness variations within QWs. The experiments were performed at 200 kV in the SACTEM - Toulouse (Tecnai - FEI) microscope, equipped with the image aberration corrector. The HRTEM images were taken along the $(5\bar{4}\bar{1}0)$ zone axis giving the image of (0002) planes only. The HRTEM images were analyzed using GPA Phase 3.5 (HREM Research Inc.), plug-ins for the image processing package Digital Micrograph (Gatan Inc.).

Results

Optical investigations

Fig. 1a demonstrates the PL spectra recorded at temperature of 77K of the samples dedicated for optical investigations grown at different pressures in the Aixtron epi-system. A long wavelength shift of the emission from 437 nm to 460 nm is observed with an increase in pressure from 100 mbar to 450 mbar.

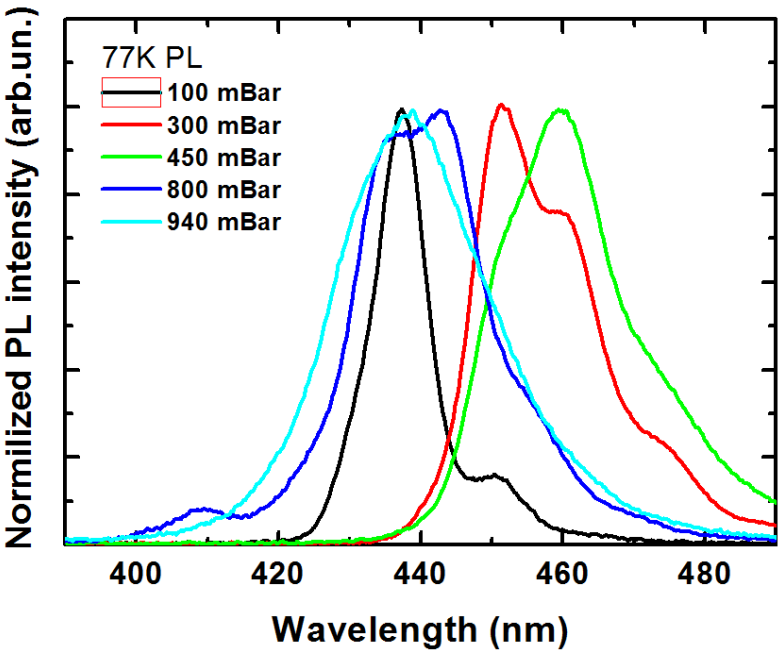

Fig. 1. PL spectra of the samples grown at different pressures in the Aixtron epi-system. An excitation wavelength is 325 nm and a current density is 20 W/cm^2.

A further pressure increase to 940 mbar leads to a shift of the emission peak position back to 440 nm. Such PL behavior might indicate a complex dependence of the In content and/or the QW thickness on a growth pressure. To explain the obtained results, the temperature dependencies of the values of the full width on a half maximum (FWHM) and the emission intensity of the PL spectra were extracted (Fig. 2).

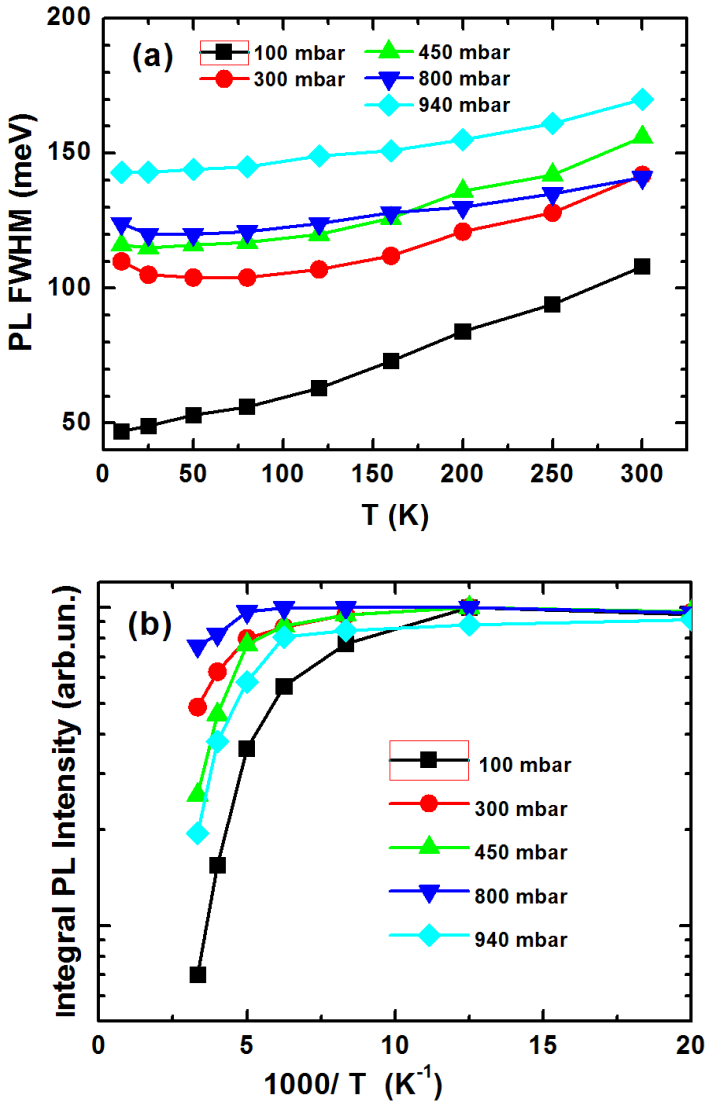

Fig. 2. Temperature dependencies of the FWHM (a) and Arrhenius plot of the PL intensity (b) obtained for the samples grown at different pressures in the Aixtron epi-system.

It is seen that whatever the recording temperature, a FWHM of the PL spectrum of the QWs grown at a higher pressure exceeds that of the QWs grown at lower one (Fig. 2a). Exceptionally, in the low temperature range, a FWHW of the PL spectra corresponding to the QWs grown at 800 mbar is slightly lower than that obtained for QWs grown at 450 mbar.

For InGaN QWs grown at 100 mbar, a monotonic increase in the FWHM in the whole temperature range is observed. Such behavior is typical for a “conventional” QW with the 2D density of states. A principle change in the temperature dependence of the FWHM of a PL spectrum, namely, a narrowing of the PL line width in the low temperature range followed by its

monotonic widening with a further temperature increase is observed for the samples with QWs grown at higher pressures. The effect is more pronounced for the QWs grown at 300mbar pressure.

Fig. 2b shows an inverse temperature dependence of the integral PL intensities obtained for this set of samples. It is seen that a maximal and a minimal drop of the intensity at elevated temperatures are observed for the QWs grown at 100 mbar and 800 mbar, respectively.

Thus, combining these data, we can conclude that an increase in pressure during the growth of InGaN layers might modify their structure in a way to create localized states in QWs hampering a lateral transport of carriers.

Structural investigations

Weak beam dark field images taken with g=2-1-10 of the active region of the structures containing the QWs grown at pressure of 100 mbar (Fig.3a) and 300 mbar (Fig. 3c) do not reveal additional dislocations there.

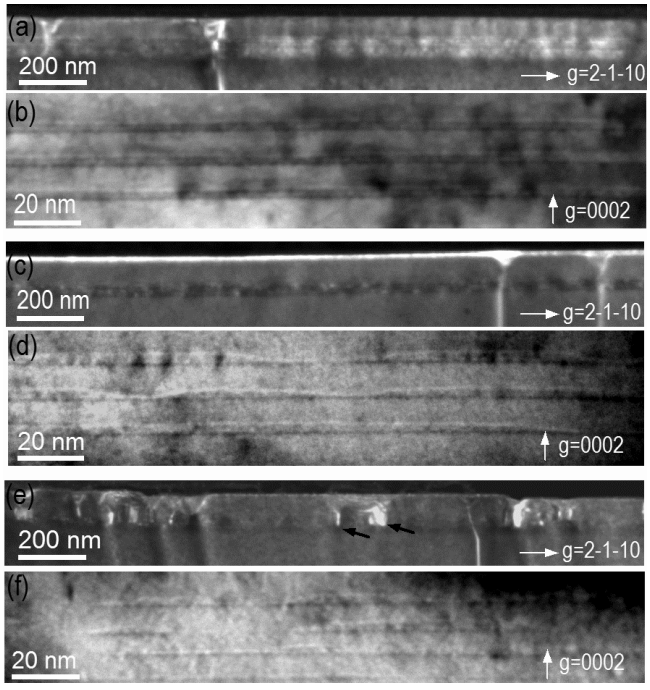

Fig.3. Cross-sectional (01-10) weak beam dark field images taken with g=2-1-10 (a), (c), (e) and dark field underfocused images taken with g=0002 (b), (d), (f) of the active region of the

structures containing QWs grown at different pressures of: (a), (b) 100 mbar; (c),(d) 300 mbar; and (e), (f) 940 mbar. Misfit defects generated at QWs are indicated by black arrows in (e).

Only threading dislocations, nucleated at the Al_2O_3/GaN interface, intersect the active regions and dissociate into V-pit defects in the subsurface GaN layer. Using standard analysis of WBDF images taken with g=0002 and g=2-1-10 (see [20] for example), the densities of mixed and edge type threading dislocations were found to be equal to (2-4)x10^8 cm^{-2} and (4-6)x10^8 cm^{-2}, respectively. In addition to these dislocations, new threading dislocations appear in the active region of the structure grown at 940 mbar (Fig. 3e, marked by black arrows) nucleating either at the first, the second or the third InGaN layer, and propagating towards the surface. A detailed analysis of their contrast at different imaging conditions (not shown here) allowed identifying these defects as pure edge type dislocations of the V-shape being similar to those described in [21]. The density of these dislocations equals (6-12) x10^9 cm^{-2}.

Cross-sectional (01-10) dark-field underfocused images of these three structures taken with g=0002 allow visualizing a morphology of the corresponding QWs (Fig. 3b,d,f). The InGaN layers grown at the lowest pressure have a quasi-constant thickness of 2.5±0.5 nm and a planar morphology (Fig. 3b).

The InGaN layers grown at elevated pressures present in form of laterally connected islands. The lateral size of islands formed during the growth at pressure of 300 mbar varies from 50 to 200 nm and their height is of 3±0.5 nm (Fig. 3d). The islands formed at the 940 mbar growth pressure are smaller in both the vertical and the lateral dimensions. Their lateral size varies from 17 nm to 70 nm while their height reaches a maximum value of 2.0 ±0.5 nm.

The GPA of the HRTEM images corresponding to these three structures allowed extracting the maps of the out-of-plane strain relative to GaN, ε_{zz}^{GaN} obtained with a spatial resolution of 1 nm (Fig. 4). The InGaN QWs appear in red and yellow colours in these images while the GaN matrix (taken as a reference) appears in green colour.

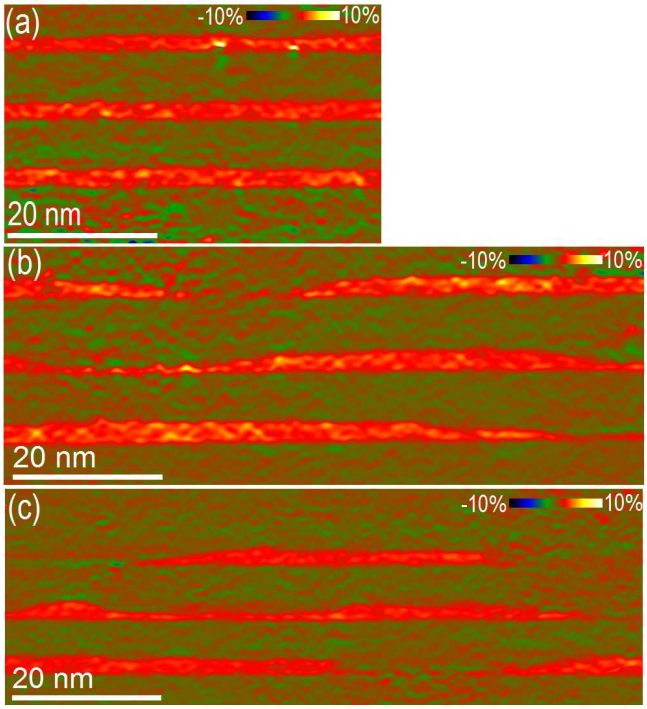

Fig. 4 Map of the out-of-plane strain relative to GaN, ε_{zz}^{GaN} obtained by geometric phase analysis of HRTEM images with a spatial resolution of 1 nm in the active region of the structures containing QWs grown at different pressures of: (a) 100 mbar; (b) 300 mbar; (c) 940 mbar.

Firstly, these maps indicate the transformation of the planar QW morphology to the island like one with an increase in the QW growth pressure. This finding is similar to what was detected during the DF image analysis. Secondly, a quantitative analysis of the strain in three QWs presenting at different depths in the same structure allowed concluding their similarity. Thus, for each structure, we have averaged different strain profiles obtained in the vertical direction *z* across the QWs presenting at different depths and extracted a strain profile characterizing an “average” QW grown at the given pressure. The out-of-plane strain profiles of the “average” QWs grown at 100 mbar, 300 mbar and 940 mbar pressures are presented in Fig. 5.

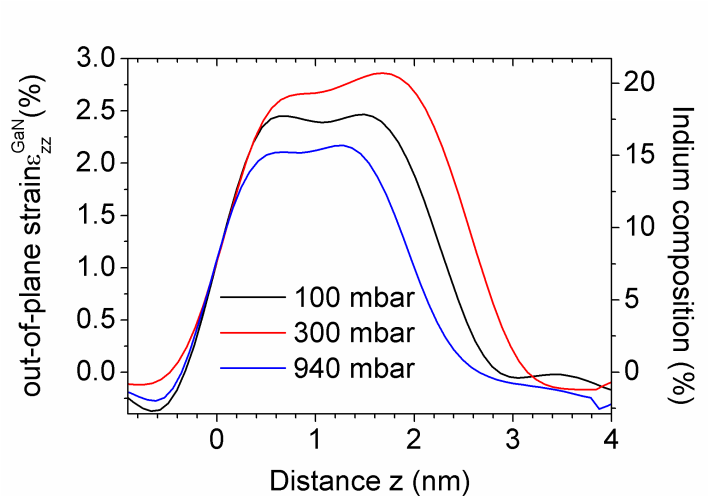

Fig. 5 Out-of-plane strain ε_{zz}^{GaN} profiles across an "average" QW grown at pressure of 100 mbar (black line), 300 mbar (red line) and 940 mbar (blue line). The right axis corresponds to indium composition within the QWs calculated from ε_{zz}^{GaN} values being corrected for a thin foil relaxation effect.

The maximum values of the out-of-plane strain in the three "average "QWs are different and equal 2.3%, 2.7% and 2.0 % for the QWs grown at 100 mbar (Fig. 5, black line), 300 mbar (Fig.5, red line) and 940 mbar (Fig. 5, blue line), respectively. The thicknesses of the "average" QWs are also different and equal 2.3 nm, 2.6 nm and 2.0 nm for the QWs grown at 100 mbar, 300 mbar and 940 mbar, respectively.

A chemical composition within the "average" QWs has been estimated from the strain profiles corrected for a thin foil relaxation effect using finite element method simulation (right axis in Fig. 5). These calculations indicate that the QWs grown at 100 mbar, 300 mbar and 940 mbar have indium composition of (17 ±1) %, (20 ±1) % and (15 ±1) %, respectively.

Electroluminescence investigations of LED structures

Figure 6 shows the dependencies of the FWHM and the peak position of the EL spectra (Fig.6a), and the external quantum efficiencies (EQE) of LED structures (Fig. 6b) on QW growth

pressure obtained for two sets of samples grown in different systems: Aixtron 2000HT and Dragon 125.

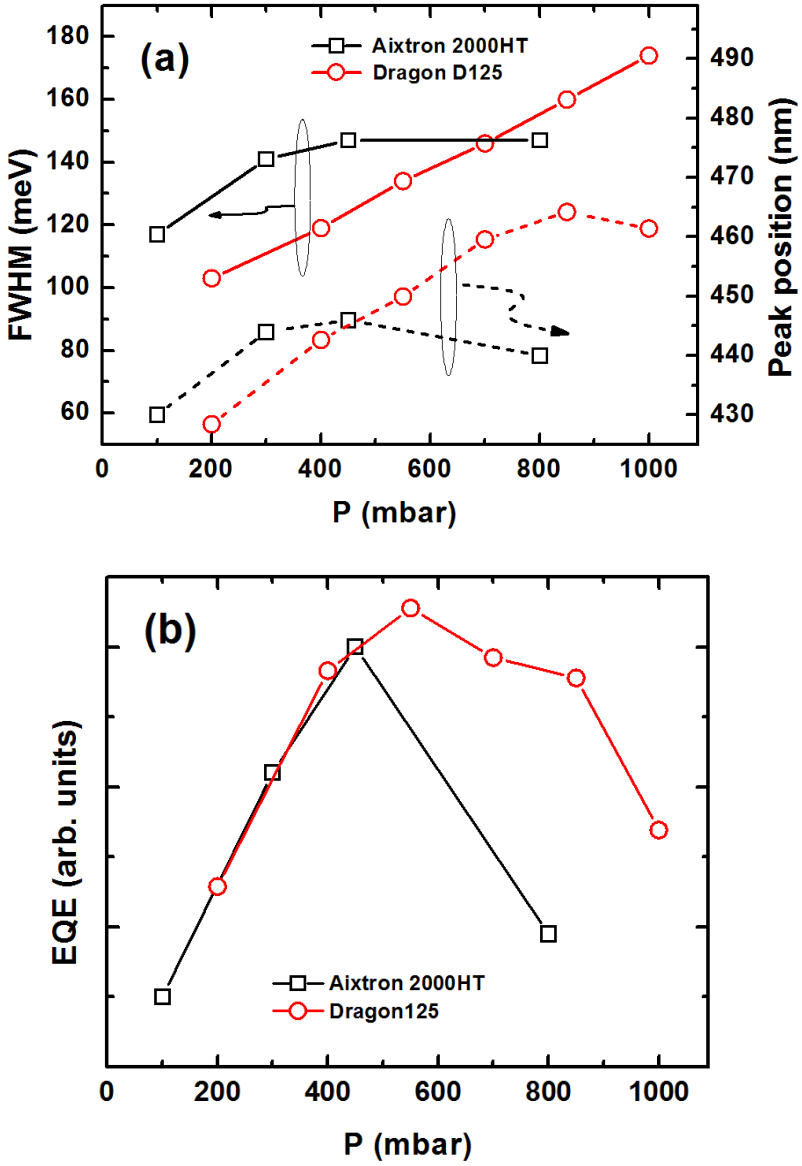

Fig. 6. EL spectrum FWHM and peak position (a) and EQE of LED structures grown in different systems: Aixtron 2000HT and Dragon 125 (b) as function of QW growth pressure.

The LED structures grown in both systems exhibit similar tendencies for the evolution of these three characteristics with an increase in QW growth pressure. The higher QW growth pressure is, the wider the FWHM of the EL spectrum (Fig. 6a, left axis). An emission peak position shifts towards longer wavelength values with an increase in pressure up to a certain

value (Fig. 6a, right axis). A further increase in QW growth pressure gives rise to the reverse shift of the EL peak position back to shorter wavelength values. The same tendency is observed for the dependencies of the EQE on pressure: the EQE increases then decreases with a continuous increase in pressure.

Despite the similarity, the growth of LED structures in the Dragon 125 system allows reaching the broader emission with the longer wavelength peak position and the higher EQE at elevated QW growth pressures with respect to that provided by the LED structures grown in the Axitron 2000HT system.

Discussion

The observed tendencies in the evolution of the PL and EL properties of the studied structures can be explained now in combination with the data on a QW average thickness, composition and morphology obtained as function of a QW growth pressure. The QWs grown at the “standard” lowest pressure of 100 mbar exist in form of two-dimensional layers with a constant thickness and composition. This structure is considered as a reference. The continuous red shift of the PL and EL peak position with an increase in a QW growth pressure from 100 mbar towards moderated values is induced by an increase in the QW thickness and composition. A concomitant emission spectra broadening is attributed to a change in the morphology of emitting sources. The InGaN QWs deposited at elevated pressures take the form of islands dispersed in lateral and vertical size, rather than the form of two-dimensional layers found in the reference structure. The overall gain in the emission intensity or EQE of LED structures containing islands can be related to a better lateral carrier confinement within three-dimensional islands than that provided by a planar two-dimensional QW. A further increase in the QW growth pressure gives rise to shrinkage of islands dimensions and a decrease in their composition. As a result, the emission peak position is inversely shifted back to the values similar to that of the reference structure. The structures with QWs grown at very high pressures

demonstrate a rapid drop in the integral PL intensity with an increase in recording temperature or a relatively low EQE. These phenomena are both related to an overall decrease of the emitting matter and to the formation of additional dislocations in the active regions. The latter can be attributed to an amplification of the parasitic reactions during a growth at elevated pressures.

The results obtained for AIX2000HT and Dragon 125 systems indicate an existence of an optimal QW growth pressure, inherent to each particular growth system, which allows reaching a longer wave emission with a maximal EQE higher than that provided by QWs grown at "standard" low pressure. We demonstrate here that a value of the optimal pressure is higher for the Dragon 125 system than for the Axitron 2000HT one. As a consequence, the LED structures grown in the Dragon 125 system provide the highest EQE even in the long wavelength emission range.

Conclusions

The effect of growth pressure on the structural, optical and electrical properties of InGaN/GaN QWs was investigated. It was shown that a growth of QWs at elevated pressures stimulates a phase separation in the InGaN QWs leading to the formation of islands. Provided that pressure is not too high, this morphological transformation is accompanied by a long wavelength shift of the emission peak position, a broadening of emission spectra and an increase in the emission efficiency with respect to properties of a "standard" QW grown at low pressure. A further increase in growth pressure gives rise to an inverse shift of the emission peak position and a loss in the structure emission efficiency. We demonstrate that an optimal QW growth pressure, which allows reaching the longest wavelength emission with a maximal EQE, is dependent on the particular growth system. The observed behavior of the morphological, compositional and emission properties of the structures in the whole studied range of QW growth pressures is related to two competing phenomena taking place during a deposition of

InGaN at elevated pressures, namely an enhanced incorporation of indium in InGaN three-dimensional islands, and an amplification of parasitic reactions on the InGaN surface.

Acknowledgments

This work has been supported by European Union Seventh Framework Program (FP7/2007-2013) under grant agreement N. 318388, RFBR foundation (grant 14-02-0052114), by Program of the Presidium of Russian Academy of Science and by the French National Research Agency under the "Investissement d'Avenir" program reference No. ANR-10-EQPX-38-01.

References

1 T. Asano, K. Yanashima, T. Asatsuma, T. Hino, T. Yamaguchi, S. Tomiya, K. Funato, T. Kobayashi, M. Ikeda, Phys. Stat. Sol. A 176, 1999, 23.

2 P. Fini, X. Wu, E. J. Tarsa, Y. Golan, V. Srikant, S. Keller, S. P. Denbaars and J. S. Speck, Jpn J Appl Phys 37, 1998, 4460.

3 A. Watanabe, H. Takahashi, T. Tanaka, H. Ota, K. Chikuma, H. Amano, T. Kashima, R. Nakamura, I. Akasaki, Jpn. J. Appl. Phys. 38, 1999, L1159.

4 D. D. Koleske, A. E. Wickenden, R. L. Henry, M. E. Twigg, J. Crystal Growth 242, 2002, 55.

5 G. Parish, S. Keller, S. P. Denbaars and U. K. Mishra, Journal of Electronic Materials 29, 2000, 15.

6 J. Selvaraj, L. Selvaraj, T Egawa, Jpn. J. Appl. Phys. 48, 2009, 121002.

7 Y. Kangawa, T. Ito, A. Koukitu and K. Kakimoto, Jpn. J. Appl. Phys. 53, 2014, 100202.

8 M. Leszczynski, R. Czernecki, S. Krukowski, M. Krysko, G. Targowski, P. Prystawko, J. Plesiewicz, P. Perlin, T. Suski, J. Cryst. Growth 318(1), 2011, 496.

9 I-hsiu Ho and G. B. Stringfellow, Appl. Phys. Lett. 69, 1996, 2701.

10 A. Koukitu, N. Takahashi, T. Taki, H. Seki, Jpn. J. Appl. Phys. 35, 1996, L673.

11 S. Yu. Karpov, MRS Internet Journal of Nitride Semiconductor Reseach, 3, 1998, 16.

12 D. Iida, K. Nagata, T. Makino, M. Iwaya, S. Kamiyama, H. Amano, I. Akasaki, A. Bandoh, T. Udagawa, Applied Physics Express 3, 2010, 075601.

13 A. Strittmatter, L. Reimann, R. Seguin, S. Rodt, A. Brostowski, U.W. Pohl, D. Bimberg, E. Hahn, D. Gerthsen, Journal of Crystal Growth, 272, 2004, 415.

14 Z. Qin, Z. Chen, Y. Tong, S. Lu and G. Zhang, Applied Physics A: Materials Science & Processing, 74, 2000, 655.

15 D Kim, Y. Moon, K.Song, I.Lee, and S. Park, Journal of Electronic Material, 30, 2001, 99.

16 C.G. Park, G.H. Gu, B.H. Lee, D.H. Jang, Ultramicroscopy 127, 2013, 114.

17 E.A. Armour, D. Byrnes, R.A. Arif, S.M. Lee, E.A. Berkman, G.D. Papasouliotis, C. Li, E.B. Stokes, R. Hefti, P. Moyer MRS Proceedings, 1538, 2013, 341.

18 W.V. Lundin, A.V. Sakharov, A.F. Tsatsulnikov, V.M. Ustinov. Semicond. Sci. Technol. 26(1), 2011, 014039.

19 M. Hytch, E. Snoeck, R. Kilaas, Ultramicroscopy 74, 1998, 131.

20 V. S. Kopp, V. M. Kaganer, M. V. Baidakova, W. V. Lundin, A. E. Nikolaev, E. V. Verkhovtceva, M. A. Yagovkina, N. Cherkashin, J. Appl. Phys. 115(7), 2014, 073507.

21 M. Zhu, S. You, T. Detchprohm, T. Paskova, E. A. Preble, D. Hanser, C. Wetzel, Phys. Rev. B 81, 2010, 125325.